IEEE Photonics Journal
An IEEE Photonics Society Publication

Open Access

Nanoscale Low Crosstalk Photonic Crystal Integrated Sensor Array

Volume 6, Number 1, February 2014

Daquan Yang
Huiping Tian
Yuefeng Ji

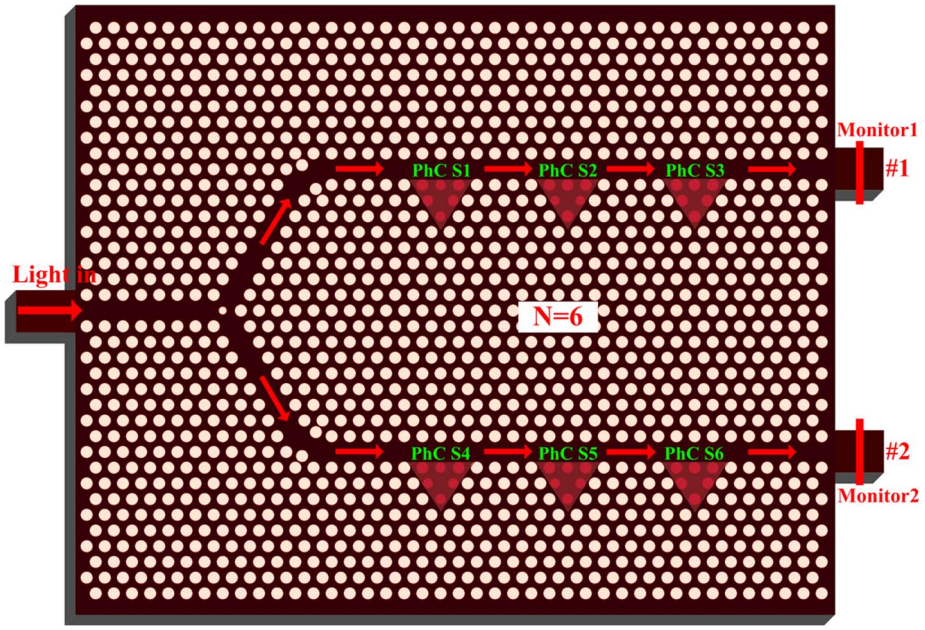

DOI: 10.1109/JPHOT.2014.2302805
1943-0655

IEEE photonics SOCIETY

IEEE

Nanoscale Low Crosstalk Photonic Crystal Integrated Sensor Array

Daquan Yang,[1,2] Huiping Tian,[1] and Yuefeng Ji[1]

[1]State Key Laboratory of Information Photonics and Optical Communications, School of Information and Communication Engineering, Beijing University of Posts and Telecommunications, Beijing 100876, China
[2]School of Engineering and Applied Sciences, Harvard University, Cambridge, MA 02138 USA

DOI: 10.1109/JPHOT.2014.2302805

Manuscript received December 31, 2013; revised January 21, 2014; accepted January 22, 2014. Date of publication January 27, 2014; date of current version February 3, 2014. This work was supported in part by NSFC under Grant 61372038, by the National 973 Program under Grant 2012CB315705, by the National 863 Program under Grant 2011AA010305, by the Fund of State Key Laboratory of Information Photonics and Optical Communications (Beijing University of Posts and Telecommunications), and by the BUPT Excellent Ph.D. Students Foundation, China, under Grants CX201212 and CX201331. The work of D. Yang was supported by the China Scholarship Council (CSC) under Grant 201206470026.
Corresponding author: D. Yang (e-mail: yangdq5896@163.com).

Abstract: We theoretically investigate a flexible design of building nanoscale photonic crystal (PhC) integrated sensor array with low crosstalk. The proposed device consists of array of side-coupled PhC resonant cavities with high Q-factors over 2×10^3. The extinction ratio of well-defined single resonance exceeds 30 dB. Each resonant cavity has different resonant wavelengths and independently shifts its resonance in response to the refractive index variations. With three-dimensional finite-difference time-domain (3D-FDTD) method, simulation results demonstrate that the proposed sensor array is desirable to perform monolithically integrated sensing and multiplexed detection. Particularly, the design method here makes it possible to effectively enhance sensor array integration density and simultaneously restrain crosstalk between each other adjacent sensors. The refractive index sensitivity of 100 nm/RIU and the crosstalk lower than -4 dB are observed, respectively. Both the specific result and the general idea are promising in future optical multiplexed sensing and nanophotonic integration.

Index Terms: Photonic crystals, integrated nanophotonic, sensors, crosstalk, waveguides.

1. Introduction

Optofluidics, referring to a class of optical systems that are synthesized with microfluidics, is an emerging technology for synthetic/analytical chemistry and nanobiotechnology. Here, light is used for controlling and efficiently analyzing fluids, colloidal solutions, and solids in a fluid, in micro-scale devices such as labs-on-chip [1], [2]. Optical sensors are the fundamental elements of optofluidics. Miniaturization of label-free optical sensors is of particular interest for realizing ultracompact lab-on-chip applications with dense array of functionalized spots for multiplexed sensing, that may lead to portable, low cost and low power devices. Over the past decades, numerous different micro optical sensors have been developed such as surface plasma resonance (SPR) sensors [3], [4], resonant cavity sensors [5], [6], whispering gallery mode sensors [7], [8], interferometric sensors [9], [10], and photonic crystal (PhC) sensors [11]–[26]. Among all these different sensors mentioned above, PhC sensors as a new type of sensors have attracted a great deal of attention in recent years. Since PhC

sensors are approximately three orders of magnitude less than commercial integrated-optic sensors [12], they become a premium choice when high sensitivity and ultra-compact size are required.

Recently, PhC sensors based on various two-dimensional (2D) PhC microcavities [13]–[26] are extensively studied. PhC sensors have 2D photonic-band gap microcavity with high quality (Q) factor and small volume (V). This can enhance the interaction between the analyte and incident photons and sensitivity to bulk properties [27]. However, most of these designs exhibit two limitations that prevent them from being applicable to real systems: 1) they typically operate as point or single sensor; 2) the number of targets which can be screened for at one time is relatively small.

To overcome these limitations and realize multiple sensing sites, PhC and PhC fiber based array sensors have been developed. Wang *et al.* [12] developed a theoretical model of the integrated parallel self-collimation sensor array; Mandal *et al.* [17] presented a nanoscale opto-fluidic sensor array based on a silicon waveguide with a 1D PhC microcavity that lies adjacent to the silicon waveguide; Yang *et al.* [18] theoretically investigated the performance of nanoscale PhC integrated sensor array on monolithic substrates using side-coupled resonant cavity array; and Sevilla *et al.* [19] proposed a photonic crystal fiber sensor array based on modes overlapping. However, in the Ref. [12], only 3 sensors are integrated on the monolithic platform. The integration density is not high enough. In the Ref. [17], sensor array consists of a silicon waveguide with a 1D PhC microcavity, which is realized on many separate silicon strips, rather than a monolithic silicon slab, and limits the enhancement of integration density. In addition, the extinction ratio of single notch of 1D photonic crystal microcavity in the Ref. [17] is only $4 \sim 10$ dB. While to the Ref. [18], when the number of sensors integrated on the monolithic platform is large, the spacing of the frequency peak of adjacent cavity is not wide enough. The sensing signal of each cavity may interact with each other due to the crosstalk in multi-cavity parallel sensing. And if the variation of one output signal caused by the refractive index (RI) change is too large, the resonance shift may be greater than the resonance spacing of adjacent resonant cavity. This will result in difficulties in recognizing the sensing signals from different cavities.

In this paper, we introduce a flexible design of building nanoscale PhC integrated sensor array with low crosstalk. The proposed sensor array consists of array of *side-coupled PhC resonant cavities with high Q-factors over* 2×10^3. Each resonant cavity has different resonant wavelength and independently shifts its resonance in response to the refractive index (RI) variations. Here, the extinction ratio of well-defined single resonance exceeds 30 dB. By using three dimensional finite difference time domain (3D-FDTD), the sensitivity of 100 nm/RIU is achieved. Simulation results demonstrate that the proposed sensor array are desirable to perform monolithically integrated sensing and multiplexed detection. When n sensors are set in cascades, the output transmission of the series exhibits n dips. The dips are independent from each other, thus a shift in one of them does not perturb others. This allows the implementation of simple but functional PhC integrated array sensors, and eventually of more complex sensor networks. In addition, we also make a thorough presentation of the simulation results on crosstalk. The crosstalk between each other sensors lower than -4 dB is observed. The results demonstrate that the design method here makes it possible to effectively restrain crosstalk of the sensors on the monolithic integration platform.

2. PhC Parallel Resonant Cavities Design

In order to efficiently enhance the integration density of sensor array and restrain crosstalk, we proposed a PhC parallel resonant cavities design, as shown in Fig. 1. The device is composed of two resonant cavities (H0-cavties) [28]–[30] side-coupled to parallel output waveguides of an optimized PhC beam-splitter $(r_1 = 0.206a, r_2 = 0.32a, dx = 0.26a)$. The PhC consists of triangular lattice air cylinders etched in silicon with the refractive index 3.46 $(n_{si} = 3.46)$. The radius of the air cylinders $r = 0.32a$, where a is the lattice constant $(a = 430$ nm$)$. The thickness of the silicon slab $T = 0.55a$. We analyze the transmission and field distribution by using the open source FDTD software Meep [31]–[33]. During the simulations, the resolution is set to be 20, namely, with the computed grid size of $a/20$. And one-spatial unit thick perfectly matched layer (PML) absorbing boundary conditions are applied surrounding the simulated domain.

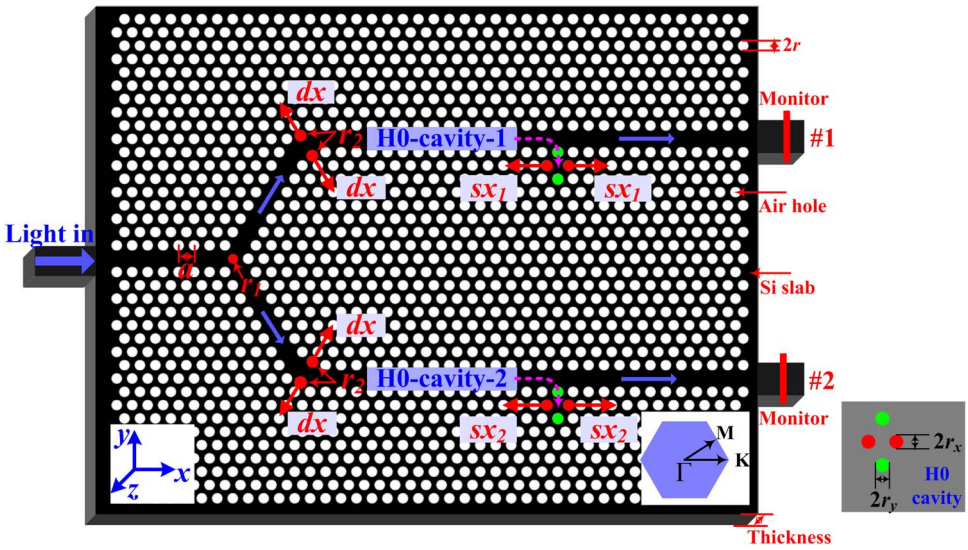

Fig. 1. Schematic of PhC parallel resonant cavities, which are composed of two H0-cavties side-coupled to parallel output waveguides of an optimized beam-splitter. Here, $a = 430$ nm, $r = 0.32a$, $r_1 = 0.206a$, $r_2 = 0.32a$, $dx = 0.26a$, and $T = 0.55a$.

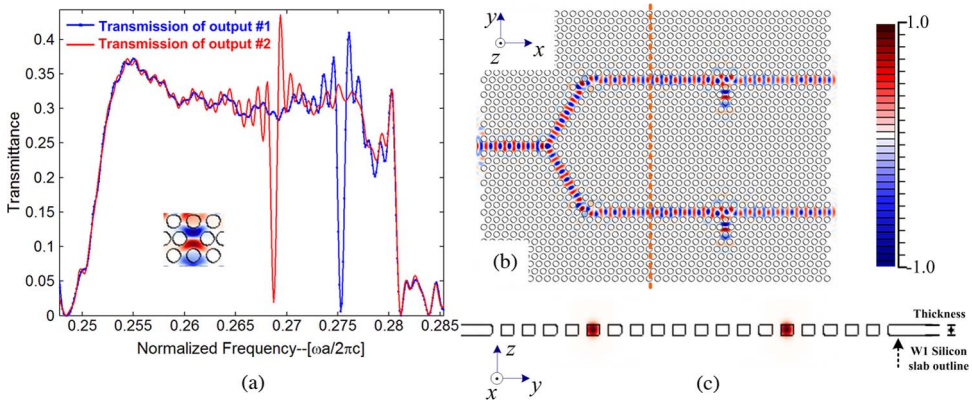

Fig. 2. (a) 3D-FDTD transmission spectra for PhC parallel resonant cavities. $sx_1 = 0.19a$, $sx_2 = 0.20a$, $r_x = r_y = 0.32a$. (b) Steady state electric field profile for the fundamental TE-like mode propagation in (b) the $x-y$ plane and (c) the $y-z$ plane (the cross section at orange dash line) with the operating frequency $\omega_0 = 0.27(2\pi c/a)$.

As seen in Fig. 1, the parameters of side-coupled cavities *are* $sx_1 = 0.19a$, $sx_2 = 0.20a$, $r_x = r_y = 0.32a$, respectively. By using 3D-FDTD method, the calculated transmission spectra and field profile of TE-like polarized lightwave are obtained, as shown in Fig. 2. As seen in Fig. 2(a), the proposed PhC parallel resonant cavities exhibit two single and narrow dips in the transmission spectra. *And the extinction ratio of the well-defined single notch exceeds 30 dB. The calculated Q-factor as high as 2700 can be observed* [18]. As seen in Fig. 2(b) and (c), the TE-like polarized light is confined strongly in both in-plane direction and out-plane direction. There is also light confinement within the side-coupled cavities. Relative to the evanescent field at the side walls of the nanocavity, we observe that the inner most holes of the side resonant cavity have a stronger optical field. This causes the resonant cavity to be very sensitive to refractive index changes due to the large degree of light-matter interaction.

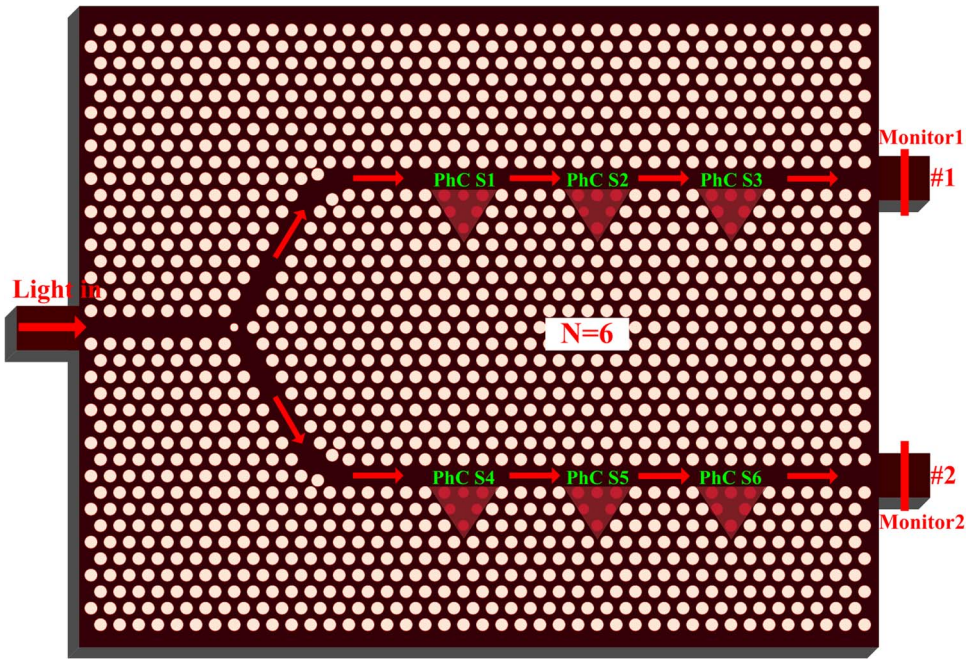

Fig. 3. Schematic of nanoscale PhC integrated sensor array on monolithic substrate. Under the red triangle shadow area there are six functionalized air holes used to be sensing area ($N = 6$).

3. PhC Integrated Sensor Array Design

Based on PhC parallel resonant cavities design mentioned above, nanoscale PhC integrated sensor array on monolithic substrate is demonstrated in Fig. 3. The proposed device consists of two parallel resonant cavity arrays, which are side-coupled to output waveguide of an optimized beam-splitter. In each branch, there are three PhC resonant cavity sensors connected in series, respectively. When n sensors are set in cascade, the transmission of the series exhibits n dips. The dips are independent of each other, thus a shift in one of them does not perturb the others. This allows the implementation of simple but functional PhC integrated sensor array, and eventually of more complex optical integrated circuits (OICs) and integrated optical devices.

As seen in Fig. 3, each side-coupled sensor unit is designed slightly differently. The specific structural parameters of each sensor unit are as follows: PhC-S1: $sx = 0.205a$, $rx = 0.30a$, $ry = 0.28a$; PhC-S2 : $sx = 0.195a$, $rx = 0.26a$, $ry = 0.32a$; PhC-S3 : $sx = 0.20a$, $rx = ry = 0.32a$; PhC-S4 : $sx = 0.20a$, $rx = ry = 0.28a$; PhC-S5 : $sx = 0.195a$, $rx = 0.28a$, $ry = 0.30a$; PhC-S6 : $sx = 0.24a$, $rx = ry = 0.32a$. The holes under the red shadow area are named as functionalized holes, used to be sensing area.

With 3D-FDTD, Fig. 4(a) illustrates the typical output transmission spectra of the TE-like polarized light. As expected, there are six deep narrow dips in the output transmission spectra. On a monolithic of PhC n resonant cavity sensors can be integrated and all of them can be interrogated simultaneously. Thus, multiplexed sensing can be realized straightforward via this method. Fig. 4(b) shows the electric field distribution for the fundamental TE-like mode propagation in the proposed PhC integrated sensor array.

4. RI Sensitivity Discussion

To investigate the refractive index (RI) sensitivity of the proposed PhC integrated sensor array, each sensor unit is independently subjected to the RI variations in the sensing area. Fig. 5(a) shows the composed transmission spectra of up-branch when one sensor is under the RI changes and the others are not. As seen, the shift in only one dip is evident while the other dips remain completely

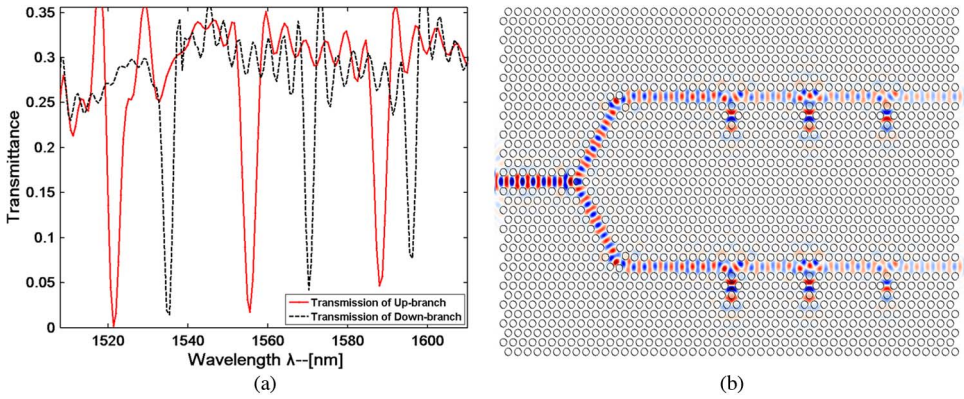

Fig. 4. (a) 3D-FDTD transmission spectra for nanoscale PhC integrated sensor array, observed when six sensor units are integrated on monolithic platform. (b) Electric field distribution for the fundamental TE-like mode propagation in PhC integrated sensor array.

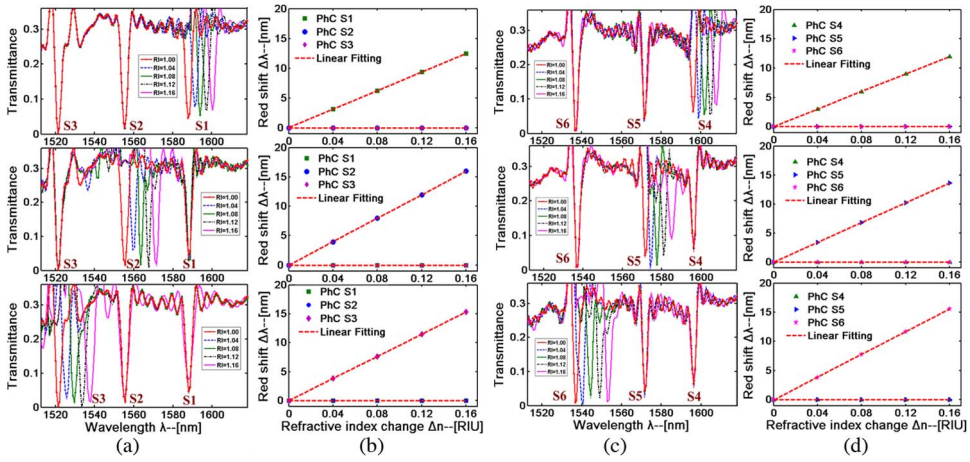

Fig. 5. (a) 3D-FDTD transmission spectra of the up-branch PhC integrated sensor array (PhC-S1, PhC-S2 and PhC-S3) when one sensor is under refractive index variations and the others are not. (b) Red shift in the resonant wavelength as a function of the refractive index increases. (c) 3D-FDTD transmission spectra of the down-branch PhC integrated sensor array (PhC-S4, PhC-S5 and PhC-S6) when one sensor is under refractive index variations and the others are not. (d) Red shift in the resonant wavelength as a function of the refractive index increases.

unchanged. And it reveals that the spectral position of the resonating dip detected at the end of output waveguides shifts towards longer wavelengths (red-shift) as the RI value is increased, *which is in good agreement with the previous works* [17], [18]. Fig. 5(b) shows resonance shift of each sensor unit (PhC-S1, PhC-S2 and PhC-S3) in the up-branch waveguide as a function of the RI variations. The composed transmission spectra of the down-branch waveguide are shown in Fig. 5(c). Fig. 5(d) shows the resonance shift of each sensor unit (PhC-S4, PhC-S5 and PhC-S6) in the down-branch waveguide as a function of the RI variations.

Here in order to quantitatively analyze the RI sensitivity of the PhCs NIASs, we choose the sensitivity by observing the shifts in the resonant wavelength of the sensor as a function of the RI variations. The resonant wavelength shift $(\Delta\lambda)$ is a function of the RI variations (Δn) in the sensing area. The sensor's RI sensitivity is expressed as follow:

$$S = \Delta\lambda/\Delta n \tag{1}$$

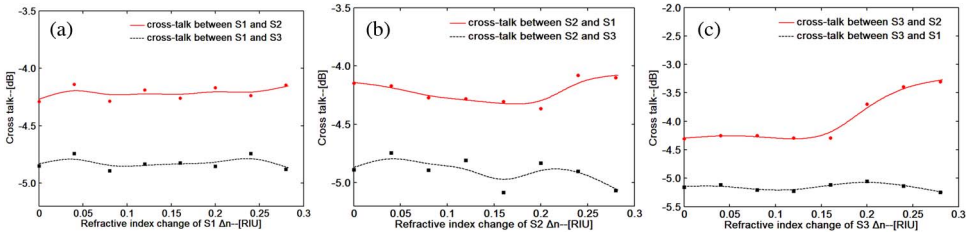

Fig. 6. The crosstalk between each other adjacent sensor units in the proposed sensor array when (a) PhC-S1, (b) PhC-S2, and (c) PhC-S3 is under the refractive index variations, respectively, and other sensors are not.

From the simulation results shown in Fig. 5, the calculated RI sensitivities of the proposed PhC integrated sensor array of $S_1 = 78.01$ nm/RIU, $S_2 = 100.06$ nm/RIU, and $S_3 = 95.76$ nm/RIU, $S_4 = 69.63$ nm/RIU, $S_5 = 84.98$ nm/RIU, and $S_6 = 97.48$ nm/RIU, are observed, respectively.

5. Crosstalk Discussion

In this section, we will discuss the crosstalk between each sensor unit by performing a detailed simulations and calculations. Here, the crosstalk calculation is defined as follow:

$$\eta_{crosstalk} = 10 \times \lg \frac{1 - A_i}{1 - A} \tag{2}$$

where A is the transmission minimum value of resonant dip of one sensor at the resonant frequency Ω. A_i represents the transmission value of the other adjacent sensors at the same resonant frequency ω when RI changes, e.g. from RI = 1.00 to 1.16. The calculated crosstalk between each sensor in the up-branch (PhC-S1, PhC-S2 and PhC-S3) is shown in Fig. 6. The crosstalk is calculated when one sensor is exposed to RI variations and the others are not. As seen in Fig. 6, the crosstalk between each other adjacent sensor units in the proposed PhC sensor array lower than -4 dB is observed.

However, when the quantity of side-coupled sensor units is large, the resonance spacing of adjacent sensor will not be wide enough. Thus, the sensing signal may interact each other easily. In addition, if the shift of one output signal caused by the RI variation is too large, the resonance shift may be greater than the resonance spacing of adjacent sensors. This will make the sensing signal detection and recognition difficult, and also restrict the distribution of the sensors on the monolithic platform. In order to overcome this drawback, we will optimize our PhC integrated sensor array device to achieve high integration density and low-crosstalk simultaneously in our future work.

6. Conclusion

In summary, by using 3D-FDTD, we have theoretically demonstrated a flexible design of nanoscale PhC integrated sensor array with high sensitivity and low crosstalk. It is important to point out that the demodulation of the PhC integrated sensor array is straightforward. When *n* sensors are set in cascades, the output transmission of the series exhibits *n* dips. And the dips are independent from each other. Thus, the proposed PhC integrated sensor array is desirable to perform monolithically integrated sensing and multiplexed detection. This allows the implementation of simple but functional PhC integrated sensor array, and eventually of more complex sensor networks. In addition, the proposed sensor array makes it possible to enhance integration density and restrain crosstalk simultaneously.

References

[1] D. Psaltis, S. R. Quake, and C. Yang, "Developing optofluidic technology through the fusion of microfluidics and optics," *Nature*, vol. 442, pp. 381–386, Jul. 2006.
[2] C. Monat, P. Domachuk, and B. J. Eggleton, "Integrated optofluidics: A new river of light," *Nature Photon.*, vol. 1, pp. 106–114, 2007.

[3] R. Karlsson, "SPR for molecular interaction analysis: A review of emerging application areas," *J. Molecular Recog.*, vol. 17, no. 3, pp. 151–161, May/Jun. 2004.
[4] C. Caucheteur, Y. Shevchenko, L. Shao, M. Wuilpart, and J. Albert, "High resolution interrogation of tilted fiber grating SPR sensors from polarization properties measurement," *Opt. Exp.*, vol. 19, no. 2, pp. 1656–1664, Jan. 2011.
[5] A. B. Matsko and V. S. Ilchenko, "Optical resonators with whispering-gallery modes—Part I: Basics," *IEEE J. Sel. Topics Quantum Electron.*, vol. 12, no. 1, pp. 3–14, Jan./Feb. 2006.
[6] A. M. Armani and K. J. Vahala, "Heavy water detection using ultra-high-Q microcavities," *Opt. Lett.*, vol. 31, no. 12, pp. 1896–1898, Jun. 2006.
[7] F. Vollmer, D. Braun, A. Libchaber, M. Khoshsima, I. Teraoka, and S. Arnold, "Protein detection by optical shift of a resonant microcavity," *Appl. Phys. Lett.*, vol. 80, no. 21, pp. 4057–4059, May 2002.
[8] A. M. Armani, R. P. Kulkarni, S. E. Fraser, R. C. Flagan, and K. J. Vahala, "Label-free, single-molecule detection with optical microcavities," *Science*, vol. 317, no. 5839, pp. 783–787, Aug. 2007.
[9] B. J. Luff, J. S. Wilkinson, J. Piehler, U. Hollenbach, J. Ingenhoff, and N. Fabricius, "Integrated optical Mach–Zehnder biosensor," *J. Lightwav. Technol.*, vol. 16, no. 4, p. 583, Apr. 1998.
[10] A. Ymeti, J. Greve, P. V. Lambeck, T. Wink, S. van Hovell, T. A. M. Beumer, R. R. Wijn, R. G. Heideman, V. Subramaniam, and J. S. Kanger, "Fast, ultrasensitive virus detection using a young interferometer sensor," *Nano Lett.*, vol. 7, no. 2, pp. 394–397, Feb. 2007.
[11] J. O. Grepstad, P. Kaspar, O. Solgaard, I. Johansen, and A. S. Sudbo, "Photonic-crystal membranes for optical detection of single nano-particles, designed for biosensor application," *Opt. Express*, vol. 20, no. 7, pp. 7954–7965, Mar. 2012.
[12] Y. Wang, H. Wang, Q. Xue, and W. Zheng, "Photonic crystal self-collimation sensor," *Opt. Exp.*, vol. 20, no. 11, pp. 12 111–12 118, May 2012.
[13] C. Kang, C. T. Phare, Y. A. Vlasov, S. Assefa, and S. M. Weiss, "Photonic crystal slab sensor with enhanced surface area," *Opt. Exp.*, vol. 18, no. 26, pp. 27 930–27 937, Dec. 2010.
[14] T. W. Lu and P. T. Lee, "Ultra-high sensitivity optical stress sensor based on double layered photonic crystal microcavity," *Opt. Exp.*, vol. 17, no. 3, pp. 1518–1526, Feb. 2009.
[15] B. T. Tung, D. V. Dao, T. Ikeda, Y. Kanamori, K. Hane, and S. Sugiyama, "Investigation of strain sensing effect in modified single-defect photonic crystal nanocavity," *Opt. Exp.*, vol. 19, no. 9, pp. 8821–8829, Apr. 2011.
[16] J. Dahdah, N. Courjal, and F. I. Baida, "Analysis of a photonic crystal cavity based on absorbent layer for sensing applications," *J. Opt. Soc. Amer. B*, vol. 27, no. 2, pp. 305–310, Feb. 2010.
[17] S. Mandal and D. Erickson, "Nanoscale optofluidic sensor arrays," *Opt. Express*, vol. 16, no. 3, pp. 1623–1631, Feb. 2008.
[18] D. Yang, H. Tian, and Y. Ji, "Nanoscale photonic crystal sensor arrays on monolithic substrates using side-coupled resonant cavity arrays," *Opt. Exp.*, vol. 19, no. 21, pp. 20 023–20 034, Oct. 2011.
[19] G. A. C. Sevilla, V. Finazzi, J. Villatoro, and V. Pruneri, "Photonic crystal fiber sensor array based on modes overlapping," *Opt. Exp.*, vol. 19, no. 8, pp. 7596–7602, Apr. 2011.
[20] T. Xu, N. Zhu, M. Y.-C. Xu, L. Wosinski, J. S. Aitchison, and H. E. Ruda, "Pillar-array based optical sensor," *Opt. Exp.*, vol. 18, no. 6, pp. 5420–5425, Mar. 2010.
[21] D. Yang, H. Tian, and Y. Ji, "The properties of lattice-shifted microcavity in photonic crystal slab and its applications for electro-optical sensor," *Sensors Actuators: A. Phys.*, vol. 171, no. 2, pp. 146–151, Nov. 2011.
[22] D. Yang, H. Tian, J. Huang, and Y. Ji, "2×3 photonic crystal series-parallel integrated sensor arrays based on monolithic substrates using side-coupled resonator arrays," presented at the CLEO, San Jose, CA, USA, May 6–11, 2012.
[23] F. Fan, W. Gu, X. Wang, and S. Chang, "Real-time quantitative terahertz microfluidic sensing based on photonic crystal pillar array," *Appl. Phys. Lett.*, vol. 102, no. 12, pp. 121113-1–121113-4, Mar. 2013.
[24] W. Lai, S. Chakravarty, Y. Zou, Y. Guo, and R. T. Chen, "Slow light enhanced sensitivity of resonance modes in photonic crystal biosensors," *Appl. Phys. Lett.*, vol. 102, no. 4, p. 041111, Jan. 2013.
[25] S. Hachuda, S. Otsuka, S. Kita, T. Isono, M. Narimatsu, K. Watanabe, Y. Goshima, and T. Baba, "Selective detection of sub-atto-molar Streptavidin in 1013-fold impure sample using photonic crystal nanolaser sensors," *Opt. Exp.*, vol. 21, no. 10, pp. 12 815–12 821, May 2013.
[26] D. Yang, H. Tian, Y. Ji, and Q. Quan, "Design of simultaneous high-Q and high-sensitivity photonic crystal refractive index sensors," *J. Opt. Soc. Amer. B*, vol. 30, no. 8, pp. 2027–2031, Aug. 2013.
[27] J. S. Foresi, P. R. Villeneuve, J. Ferrera, E. R. Thoen, G. Steinmeyer, S. Fan, J. D. Joannopoulos, L. C. Kimerling, H. I. Smith, and E. P. Ippen, "Photonic-bandgap microcavities in optical waveguides," *Nature*, vol. 390, pp. 143–145, 1997.
[28] K. Nozaki, T. Tanabe, A. Shinya, S. Matsuo, T. Sato, H. Taniyama, and M. Notomi, "Sub-femtojoule all-optical switching using a photonic-crystal nanocavity," *Nature Photon.*, vol. 4, pp. 477–483, 2010.
[29] M. Notomi, "Manipulating light with strongly modulated photonic crystals," *Rep. Prog. Phys.*, vol. 73, no. 9, pp. 096501-1–096501-57, Sep. 2010.
[30] Z. Zhang and M. Qiu, "Small-volume waveguide-section high Q microcavities in 2D photonic crystal slabs," *Opt. Exp.*, vol. 12, no. 17, pp. 3988–3995, Aug. 2004.
[31] J. D. Joannopoulos, S. G. Johnson, J. N. Winn, and R. D. Meade, *Photonic Crystals: Molding the Flow of Light,* 2nd ed. Princeton, NJ, USA: Princeton Univ. Press, 2008.
[32] A. F. Oskooi, D. Roundy, M. Ibanescu, P. Bermel, J. D. Joannopoulos, and S. G. Johnson, "Meep: A flexible free-software package for electromagnetic simulations by the FDTD method," *Comput. Phys. Commun.*, vol. 181, no. 3, pp. 687–702, 2010.
[33] S. Pal, E. Guillermain, R. Sriram, B. L. Miller, and P. M. Fauchet, "Silicon photonic crystal nanocavity-coupled waveguides for error-corrected optical biosensing," *Biosens. Bioelectron.*, vol. 26, no. 10, pp. 4024–4031, Jun. 2011.